Find out how MERCK

Volume 169, Issue 1, p161–173.e12, 23 March 2017

RESOURCE

Tridimensional Visualization and Analysis of Early Human Development

Morgane Belle, David Godefroy, Gérard Couly, Samuel A. Malone, Francis Collier, Paolo Giacobini, Alain Chédotal[6]

[6] Lead Contact

Open Archive | PlumX Metrics

DOI: https://doi.org/10.1016/j.cell.2017.03.008 | CrossMark

Article Info

Highlights

- We used 3DISCO/iDISCO+ clearing methods to start building a 3D human cell atlas
- A collection of high-resolution images of whole human embryos and fetal organs
- An interactive online resource and 3D digital database of human development
- Unknown features of human development revealed in cleared and immunostained embryos

Summary

Generating a precise cellular and molecular cartography of the human embryo is essential to our understanding of the mechanisms of organogenesis in normal and pathological conditions. Here, we have combined whole-mount immunostaining, 3DISCO clearing, and light-sheet imaging to start building a 3D cellular map of the human development during the first trimester of gestation. We provide high-resolution 3D images of the developing peripheral nervous, muscular, vascular, cardiopulmonary, and urogenital systems. We found that the adult-like pattern of skin innervation is established before the end of the first trimester, showing important intra- and inter-individual variations in nerve branches. We also present evidence for a differential vascularization of the male and female genital tracts concomitant with sex determination. This work paves the way for a cellular and molecular reference atlas of human cells, which will be of paramount importance to understanding human development in health and disease.

View File

Introduction

For centuries, the intricacies of human development have remained an enigma and its study unexplored due to sociocultural, religious, and moral reasons (Morgan, 2009). In the second half of the twentieth century, a growing interest in experimental embryology and technological developments (King and King, 1986) led to the first scientific descriptions of human embryo development (His, 1881, Keibel and Elze, 1908). In the middle of the 20th century, Franklin Mall and colleagues at the Carnegie Institute collected, sectioned, and stained thousands of human embryos and fetuses (Morgan, 2009). Wax reconstructions and 3D embryo models were generated (Norman, 1923) to define stages of human embryogenesis, still in use today (Keibel and Mall, 1910, O'Rahilly and Müller, 1987). Similar collections of human embryos were initiated in other countries (Blechschmidt, 1977, Fujimoto, 2001). These data still appear in all modern textbooks and atlases of embryogenesis and developmental biology. More recently, histological sections were digitized and reconstructed in 3D (de Bakker et al., 2016). Immunohistochemical studies have also been performed but lack the 3D information, which is essential to understanding organogenesis. Ex vivo 3D images of paraformaldehyde (PFA)-fixed human embryos were recently obtained by using magnetic resonance imaging or phase-contrast X-ray radiographic computed tomography; however, the resolution is still far from being at the cellular level (Kanahashi et al., 2016, Yamada et al., 2010).

Whole mouse brains and embryos rendered transparent with various procedures can be imaged with excellent cell resolution (Richardson and Lichtman, 2015). Solvent-based clearing methods such as 3DISCO (Three-dimensional imaging of solvent cleared organs) (Ertürk et al., 2011) and its derivatives iDISCO (Renier et al.,

Hide Pane

Images/Data

Figure 1 View all Images/Data

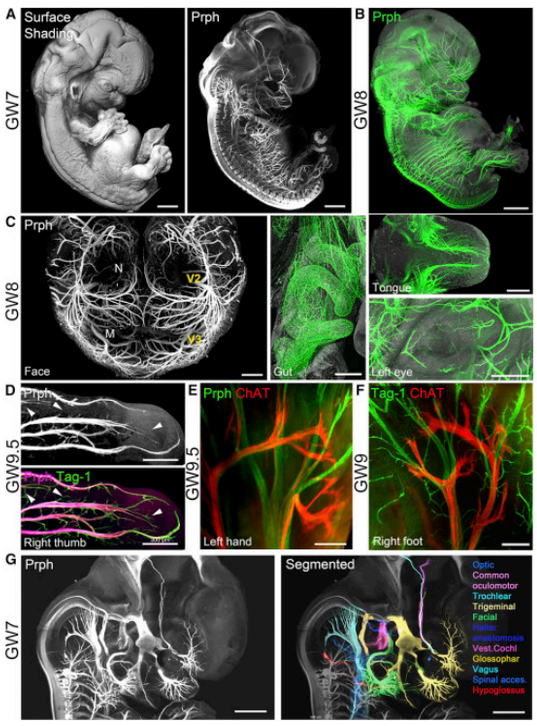

Figure 1

3D Analysis of Peripheral Nervous System Development in Human Embryos

All panels are LSFM images of solvent-cleared embryos and fetuses.

(A) Surface shading image (left) and Prph labeling of peripheral nerves (right) at GW7.

(B) Overlay of the surface shading image (gray) and Prph labeling (green) at GW8.

(C) High-magnification images of Prph+ innervation at GW8. The middle and right panels are overlays of the surface contrast image (gray) and Prph labeling (green).

(D) GW9.5 thumb labeled for Prph and Tag-1. The two markers co-localize but the thinnest branches (arrowheads) are better labeled with Tag-1.

Marketplace Recommendations

iF Design Award

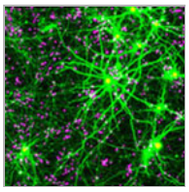
BrightCell™ Live Cell Imaging Media

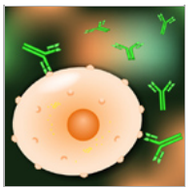
30,000+ Primary Antibodies

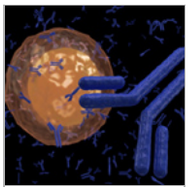
Highly Specific Anti-Tag Antibodies

Ads Powered with

Cell Career Network
Feedback
The best jobs in life science
EXPLORE MORE

2014), iDiSCO+ (Renier et al., 2016), and uDISCO (Pan et al., 2016) are fully compatible with whole-mount immunofluorescence (Belle et al., 2014, Renier et al., 2014). The rise of light sheet fluorescence microscopy (LSFM) has led to the development of imaging setups compatible with large field objectives and thick (>1 cm) specimens (Dodt et al., 2007). We set out to develop a protocol that combines antibody labeling and tissue clearing for better analyses in human embryology.

Here, we have performed whole-mount immunostaining on 36 human embryos and fetuses ranging from 6 to 14 weeks of gestation with over 70 antibodies, most of which had never been used in humans (see STAR Methods and **Table S1**). We have generated 3D images of human embryos at an unprecedented cellular resolution. This work offers a unique opportunity to start building a molecular and cellular atlas for the study of human development. The possible applications of this new method in the field of embryology are countless. They open new avenues for the study of molecular mechanisms regulating the development of human embryos in physiological and pathological conditions.

▼Results and Discussion

▼Development of the Human Peripheral Nervous System

We used a protocol for whole-mount immunostaining and 3DISCO clearing to analyze the development of human embryos (first 8 weeks of gestation) and fetuses (from 8.5 to 14 weeks, see STAR Methods). We first studied the development of the peripheral nervous system (PNS) using antibodies against the neuron-specific intermediate filament protein peripherin (Prph), which in rodents is expressed by sensory and autonomic axons (Parysek et al., 1988). In human fetuses, Prph labels auditory and vomeronasal nerves (Casoni et al., 2016, Locher et al., 2013).

We first used embryos at gestation week 6 (GW6) (or, Carnegie stage CS17, n = 1; see STAR Methods for stage determination), GW7 (CS19, n = 2), GW7.5 (CS21, n = 1), and GW8 (CS23, n = 3). As previously reported for mice (Belle et al., 2014, Renier et al., 2014), tissue-shrinkage was observed (20%–40% of its original size) and remained homogeneous throughout the embryo. This shrinkage can be avoided using iDISCO+ (Renier et al., 2016), however, the cleared embryos produced by this method are more fragile and their fluorescence less stable than with 3DISCO. In addition, the methanol treatment needed for iDISCO+ is not compatible with some antibodies. Last, the size reduction after 3DISCO allowed whole embryos to be imaged via LSFM and Prph+ peripheral nerves to be visualized from the brainstem and spinal cord to their distal extremities (Figures 1A–1C and S1A and S1B and **Movie S1**).

We next tested specific markers of sensory and motor axons, focusing primarily on the innervation of the developing feet and hands from GW6–GW12. Motor and sensory axons were respectively labeled with antibodies against choline acetyl transferase (ChAT; n = 14 cases) and transient adhesion glycoprotein-1 (Tag-1/Contactin 2; n = 22 cases) (Karagogeos et al., 1997). Double staining for Prph and Tag-1 (n = 14) confirmed that both markers overlapped in peripheral nerves, although from GW9, the thinnest axonal branches were better seen with Tag-1 (Figure 1D). In contrast, there was no overlap between ChAT+ and Prph+ (Figure 1E; n = 6) or ChAT+ and Tag-1+ (Figures 1F and S1C; n = 7) immunoreactive axons. Motor nerve roots were not immunoreactive for Prph (data not shown), suggesting that in humans, Prph is differentially expressed between spinal cord and cranial motor axons.

3D virtual dissection of organ innervation with Imaris segmentation plugins was performed to trace, artificially color, and reconstruct individual nerve fascicles (STAR Methods). This method was applied to GW7 (CS19; n = 2) and GW8 (CS23; n = 1; Figure 1G) cranial nerves (Figures 1G and S1A and **Movie S1**). Fetuses older than GW8, too large for our LSFM microscope, were dissected prior to processing in order to image limbs and other large organs.

Segmentation-based tracing was used to reconstruct the sensory innervation of the hand from GW6 to GW11.5. The human hand contains the ulnar (or cubital), median, and radial nerves, which innervate different hand areas in a pattern highly conserved between individuals (Unver Dogan et al., 2010).

Sensory nerves and their branches in the hands of 14 embryos and fetuses were reconstructed in 3D using Prph (GW7–GW11, n = 11) or Tag-1 (GW6–GW9.5, n = 3) immunostaining (Figures 2A and 2B and S1D) and used to create a developmental time-lapse of sensory innervation in the human hand (Figure 2B and **Movie S2**). Furthermore, we reconstructed the motor (ChAT+) and sensory (Tag-1+) innervation of two GW8.5 and GW9 fetuses (Figures 2C and 2D and S1C and **Movie S2**) to determine where and how the two types of nerves diverge.

We next compared the nerve branching patterns in 11 hands and found, in all individuals analyzed, striking heterogeneity between the left and right hands. At all ages, the median nerve was the most similar (Figure S2A and data not shown), whereas noticeable differences in the number and length of branches existed between the left and right ulnar or radial nerves (Figures S2A and S2B and **Movie S2**). The low number of cases analyzed did not allow for the detection of any correlation with hand laterality. Interestingly, unlike in adults, the musculocutaneaous nerve extended into the hand, at least until GW11 (Figure 2B).

The adult cutaneous innervation is topographically organized with each of the three nerves innervating non-overlapping skin territories. To determine how this map is established, we pseudo-colored the domains overlying Tag-1+ axons in hands at GW6, GW8.5, and GW11.5 (Figure S2C and **Movie S2**). At GW8.5, most of the hand

(E) Dorsal view of a GW9.5 hand double labeled for ChAT (motor axons) and Prph (sensory axons), showing the lack of co-localization.

(F) Dorsal view of a GW9 foot labeled for ChAT and Tag-1. The two markers are not co-expressed.

(G) Right view of the head and cranial nerves at GW7 (Prph staining). On the right panel, cranial nerves are segmented and highlighted with specific pseudo-colors.

Abbreviations: N, nostrils; M, mouth; V2 (maxillary) and V3 (mandibular), second and third branches of the trigeminal nerve.

Scale bars, 1,000 μm in (A) and (G), 2,000 μm in (B), 500 μm in (C), 300 μm in (D), 200 μm in (E), and 150 μm in (F).

See also Figure S1.

View Large Image | View Hi-Res Image | Download PowerPoint Slide surface was already covered with nerves whose topography appeared mature by GW11.5. The middle and index fingers are particularly interesting given that their dorsal surfaces are shared by several nerves. The median nerve, which normally only arborizes ventrally, projects to the dorsal side of these fingers. At GW6, the median nerve had not yet reached the tip of the index on the palmar (ventral) side but started to branch dorsally, ahead of the radial nerve, between future phalanges (Figure S2D). By GW8, the median nerve reached the tip of the index finger ventrally and started to cover the dorsal and distal part, whereas the radial nerve only innervated the caudal part of the dorsal side of the index finger. This pattern was unchanged at later ages (Figure S2D).

Our protocol allows 3D visualization of the development of the peripheral innervation of early human fetal stages (first trimester of life) at a high level of precision and detail and has revealed several unknown features of the development of limb innervation. First, an adult-like pattern of the domains of the skin covered by each nerve is already established during the late embryonic-early fetal period. However, within each domain, the pattern of nerve branching can be highly divergent not only between individuals but also within the same individual. This is particularly striking at the level of the hands, where the arborization of the ulnar and radial nerves significantly differ between the right and left hands. This suggests that the development of the PNS innervation is, at least to some extent, stochastic and not profoundly influenced by specific guidance cues distributed in the developing limbs and extremities (Hassan and Hiesinger, 2015). Moreover, in digits that are shared by multiple nerves there is no significant overlap of the branches originating from the different nerves. Our data infer that median nerves grow faster and start invading the dorsal part of some digits prior to the other nerves and that this may prevent them from entering these territories. Finally, significant remodeling of the sensory innervation occurs. The length of human embryogenesis, as compared to that of rodents, will facilitate the analysis of tissue remodeling during development.

Next, we further validated our method by testing a large palette of antibodies against proteins expressed by many cell types in developing mouse and human embryos (STAR Methods).

▼3D Analysis of Human Muscle Development via LSFM

The current knowledge of skeletal and head muscle development in humans is based on histological studies conducted during the first half of the twentieth century (Gasser, 1967, Gilbert, 1957) and immunostaining with a few muscle cell markers (Abe et al., 2010, De la Cuadra-Blanco et al., 2013). The distribution of muscle cell progenitors in the embryo, however, has never been reported. The transcription factor (TF) Pax7, is a muscle stem cell marker and key initiator of myogenesis in jawed vertebrates (Bryson-Richardson and Currie, 2008). We observed Pax7 immunoreactive nuclei homogenously distributed within each developing muscle of GW9.5 and GW10.5 arms and legs (Figures 3A and 3B and **Movie S3**; n = 1). As expected, all developing Pax7+ muscles were contacted by ChAT+ motor branches (Figure 3B). GW9 leg and arm (n = 1) were also triple-immunostained for ChAT, Tag-1, and myogenin (Myog), a myogenic TF expressed by differentiating myoblasts (Bryson-Richardson and Currie, 2008) (Figure 3C and **Movie S3**). This immunostaining shows that clusters of Myog expressing cells are found at the extremities of each motor nerve branch.

Doublecortin (Dcx) is an X-linked gene that encodes a microtubule-associated protein (Gleeson et al., 1998, des Portes et al., 1998). Mutations in *DCX* impede neuronal migration and cause lissencephaly. Dcx may also influence the development of the neuromuscular junction in humans (Bourgeois et al., 2015). Dcx immunostaining on limbs at GW8 (n = 1), GW9.5 (n = 1), GW10 (n = 1), GW10.5 (n = 1), and GW13.5 (n = 1) showed that developing muscles express Dcx (Figure 3D and data not shown). Sensory nerves were also immunoreactive for Dcx (Figure 3D). Myosin heavy chain (MHC) was previously detected in skeletal, heart, and craniofacial muscles from human fetuses (Abe et al., 2010). Here, we studied the distribution of MHC+ muscles throughout the body at GW8–GW14 (Figure 3E and **Movie S3**; n = 9 cases). All muscles in the upper half of a GW8 embryo (n = 1) were labeled and identified with an unprecedented resolution (Figure 3E and **Movie S3**). Whole-mount MHC muscle staining was also performed on GW11 and GW14 arms and legs (Figures S3B and S3C). Developing muscles and motor innervation could be simultaneously visualized following MHC/ChAT double immunostaining (Figure 3F and not shown), and importantly, the muscles within each hand and foot of a GW9.5 fetus could be segmented (Figures 3F and S3A and S3D and **Movie S3**). Moreover, the shape of the developing bones, which appear as black areas on optical sections, could also be extracted and visualized in 3D (Figure S3D).

▼3D Analysis of the Vasculature in Human Embryos

Existing data based on the filling of large arteries and veins (Mall, 1905), 3D reconstructions of histological sections (de Bakker et al., 2016), and vascular corrosion casting (Zawiliński et al., 2001) provide an incomplete view of the early development of human vasculature. In chicks and mice, blood vessels arise from endothelial cell progenitors (angioblasts), which aggregate to form a dense vascular meshwork covering the embryo, a process known as vasculogenesis (Chung and Ferrara, 2011). Functional continuity occurs later through the remodeling of this initial endothelial network. As the embryo grows, new vessels sprout from existing ones, in a process called angiogenesis. Here, we first performed whole-mount labeling with antibodies against plasmalemma vesicle-associated protein (Plvap; also known as PV-1 or PAL-E), a transmembrane glycoprotein expressed by fenestrated microvascular endothelial cells (Elima et al., 2005). Whole embryos at GW8 (n = 2) or various organs from GW9.5–GW14 fetuses (n = 8) were labeled and imaged with LSFM. At GW8, an extremely dense Plvap+ vascular network of endothelial cells extended throughout the body (Figure 4A and **Movie S4**), except in developing bones and corneas (Figure 4B and **Movie S4**). This supports the existence of a phase of vasculogenesis preceding angiogenesis in human embryos. Among other endothelial cell markers tested, collagen IV also labels capillaries, but less efficiently than Plvap (Figure 4C). The 3D organization of developing arteries on GW9–GW14 organs (n = 6 fetuses) were assessed with immunostaining for smooth-muscle-specific α-actin (SMA) (Figure 4D and **Movie S4**).

Mammalian lymphatic vasculature development is documented for several species (Yang and Oliver, 2014), but not much is known about human lymphangiogenesis (Sabin, 1909). The lymphatic system is crucial for immune response and understanding its development might allow us to gain some insights into some human diseases. To start investigating lymphangiogenesis in human fetuses, we next labeled the gastrointestinal tract of a GW14 fetus with antibodies against the glycoprotein podoplanin, a lymphatic cell marker (Breiteneder-Geleff et al., 1999, Schuster et al., 2015), and found many isolated podoplanin+ cells covering the gut and stomach (Figure 4E). Lymphatic cells could also be seen by using Prox-1 staining (data not shown). The lack of podoplanin+ capillaries at this age suggests that, as in other mammals, the human lymphatic system might mature later than the vascular system.

▼Lung Development in Human Embryos

In human embryos, the lung primordia and the trachea emerge from the foregut endoderm around CS11/GW4 (O'Rahilly and Müller, 1987), and airway branching proceeds from GW6 to GW16 during the pseudoglandular stage (Galambos and deMello, 2007). New bronchial branches, which bud from existing ones, further divide and lead to an expansion of the tree. Only a few immunohistological studies of human embryo lungs have been conducted (Sparrow et al., 1999). Here, we performed whole-mount immunostaining with 11 antibodies on lungs from 8 embryos and fetuses at GW8–GW14.

In the mouse, the sex determining region Y (SRY)-box 9 (Sox9) TF is expressed in alveolar epithelial cell progenitors at the distal part of each lung branch (Rockich et al., 2013), whereas Sox2 is restricted to the proximal part (Maeda et al., 2007). We observed a similar result in human lungs where all terminal bronchial buds were Sox9+ (Figures 5A–5D, 5H , and S4A and **Movie S5**), whereas Sox2 was expressed in a complementary pattern (Figures S4A and S4D). Strikingly, double staining for Sox9 and Dcx, which was not yet reported to be present in the lung epithelium, showed that Dcx was also expressed in the proximal epithelial portion of each airway (Figures 5A and 5B). We also visualized in 3D the vasculature of the lung with Plvap (Figures 5A–5C and S4B). The small capillary plexuses in the lung mesenchyme wrapping around terminal buds at GW8 are not isolated but form a continuous network with the larger vessels (Figures 5A–5C and S4B), thereby supporting an angiogenesis mode of lung vascularization as observed in mice (Parera et al., 2005).

The complete reconstruction of the mouse airway lineage revealed that the branching pattern is highly stereotyped with new branches budding according to 3 modes: domain branching (daughter branches form in a row) and planar and orthogonal bifurcation budding (Metzger et al., 2008). We performed such a lineage analysis in human whole lungs by using the segmentation of Sox9/Dcx (or Sox9/Sox2) bronchioles (Figures 5D and 5E and **Movie S5**). We observed three branching modes in humans (Figure 5E), similar to the mouse, but with some evidence of asymmetric bifurcations (Figure 5E). We next performed immunolabeling for smooth muscle markers SMA and myosin smooth muscle (MyoSM). In both cases, smooth muscles surrounding the bronchi and the proximal part of airway epithelial tubules were labeled (Figures 5F and 5G and S4A). The absence of smooth muscles on distal buds was confirmed by using Sox9 immunostaining (Figure 5H). Incidentally, smooth muscle staining also allowed to visualization of lung arteries and arterioles (Figures 5F and 5G and **Movie S5**).

The lung is primarily innervated by sympathetic and parasympathetic axons traveling through the vagus nerve. Parasympathetic ganglia also contribute to the innervation of the trachea and main bronchi (Aven and Ai, 2013). Due to the complexity of the airway tree, understanding its innervation can only be achieved in 3D. We visualized lung innervation by using immunostaining against Prph, Tag-1, and ßIII-tubulin. Immunoreactive vagus axons extended to the most distal portion of the airway branches (Figures S4C and S4D). Preliminary results indicate that the development of the vasculature of the human heart and its innervation (using immunostaining for Tyrosine hydroxylase) can also be studied with this 3D method (Figures 5I and 5K and S4E and **Movie S5**).

▼3D Analysis of Urogenital System Development in Human Embryos

In adult mammals, the urogenital system is comprised of the kidneys, urinary tracts, gonads, and reproductive ducts. Before GW7–GW8, the human gonadal ridges are undifferentiated. Genital ducts appear morphologically similar in both sexes with two paired structures: the Wolffian ducts (WDs), which are derived from the mesonephros, and the Müllerian ducts (MDs), whose differentiation is induced and guided by the WD. A major reorganization of the genital tracts accompanies sex determination (Jacob et al., 2012, Orvis and Behringer, 2007). In males, MDs regress under the influence of an anti-Müllerian hormone produced by the testes. In females, the WDs degenerate and the MDs transform into the female reproductive ducts (Georgas et al., 2015, O'Rahilly, 1983).

Knowledge of urogenital system development is primarily based on histological and electron microscopy analysis (Fritsch et al., 2012, Hashimoto, 2003) and has not yet been studied at a cellular and molecular level in humans, unlike in mice (Georgas et al., 2015, Little et al., 2007). We studied the development of the human urogenital system by using antibodies against Pax2 TF. Pax2 mRNA was previously detected in the mesonephros and WD at GW6–GW7 (Tellier et al., 2000). We used embryos and fetuses of either sex, including 11 males (GW8–GW14) and 9 females (GW7–GW14). All major components of the urogenital system were visualized in 3D (Figures 6, 7, and S5 and **Movie S6**) and individually segmented. In the youngest male embryo (GW8), the caudal tip of the MD was in close contact with the WD but had not yet fully elongated (Figures 6A and 6B), and mesonephric tubules stemming from the WD covered the testis primordium. Kidneys still occupied a ventral position adjacent to the genital ridges (Figure 6A). At GW9.5 (n = 1), the MD further elongated along the WD but did not yet join (Figures 6C and 6D). In GW10 male fetuses (n = 2), the two MD were fused and extended medially between the two WD up to the urogenital sinus. However, in both cases, the MD started to fragment dorsally (Figures 6E and 6F and Figure S5A), and this remnant of the fused MD might give rise to the prostatic utricle. At older ages, such as GW14 (n = 1), the mesonephric nephrons of the WD have regressed while the epididymis ducts and vas deferens have emerged (Figure 6G). As previously reported (Jacob et al., 2012), an apical MD remnant is still present next to the rete testis by GW14 (Figures 6G and 6J and **Movie S6**). Sox9 is essential to testes differentiation in males, and its mRNA was first detected around CS19–CS21 (GW7–GW7.5) (Hanley et al., 2000). Using whole-mount immunostaining for Sox9 on GW10, GW11, GW13.5, and GW14 fetuses (n = 1 for each), we visualized the 3D organization of the testes cords, containing Sox9+ Sertoli cells (Figure 6H and 6J, **Movie S6,** and data not shown). We also stained GW10.5–GW13 female fetuses with Pax2 (n = 6) and followed in 3D the reorganization of the urogenital tract (Figures 7 and S5). In our youngest female fetus (GW10.5) the MD have already fused to form the uterovaginal canal (Figure 7A). The WD were still continuous but mesonephric tubules began to regress. At GW11.5, the regression of the mesonephros and WD was more pronounced and the length of the two MD increased (Figure 7B). At GW13, the distal part of the WD had dissolved whereas its cranial part transformed into the Fallopian tubes (Figures 7C and S5B and **Movie S6**). The vascularization of the developing gonads is thought to play a role in their maturation (Brennan et al., 2002, Coveney et al., 2008). We performed double staining for Pax2 and Plvap to study the interaction between the vasculature and the genital tracts. Interestingly, at GW8 and GW10, the developing testes and WD were embedded in a dense capillary meshwork but the MD was avascular (Figures 7D and 7E). In contrast, in a GW10.5 female fetus, both the MD and the WD were vascularized and a dense vascular network ensheathed the MD by GW13 (Figures 7F and 7G and **Movie S6**). While we could not study younger female embryos, these results suggest that MD angiogenesis may be sex dependent. This differential vascularization of the developing MD in males and females at GW10 suggest that their regression in males, which starts around this stage, could be linked to or facilitated by the lack of vascularization. By contrast, the WD are vascularized in both sexes. Interestingly, the distal fused part of the Müllerian ducts does not seem to regress and likely gives rise to the prostatic utricle, as previously proposed (Jacob et al., 2012).

Information on the early development of human nephrons is scarce (Ludwig and Landmann, 2005). Staining of GW10–GW13.5 kidneys (n = 5) showed that Pax2 and Sox9 are both expressed in the epithelium of the ureteric tree (Figure S6). Pax2, together with another TF, Six2, was also found in nephron precursors of the cap mesenchyme surrounding the ureteric tips in the nephrogenic zone of the developing kidney (O'Brien et al., 2016). Staining of the endothelial cells with Plvap revealed the presence of developing glomeruli and their morphology (Figure S6D).

▼Transcription Factors: New Tools to Study Human Embryology

During development, cell differentiation toward specific lineages is controlled by a cascade of transcription factors. We used antibodies against 19 transcription factors to follow the development of multiple organs.

In mouse and human embryos, Sox10 is expressed by oligodendrocytes, neural crest cells, and some of their derivatives (Betters et al., 2010, Bondurand et al., 1998). *SOX10* mutations cause various diseases such as neurocristopathies, melanoma, and peripheral demyelinating neuropathies (Bondurand and Sham, 2013). Here, we performed double immunostaining for Sox10 and Prph on limbs from five fetuses, at GW9–GW12. Sox10+ cells were widely distributed throughout the PNS, at the level of the dorsal root ganglia and all along Prph-labeled nerves and branches (Figure S7A and **Movie S7**). These Sox10+ cells most likely correspond to Schwann cell precursors, which in the mouse migrate along PNS axons (Espinosa-Medina et al., 2014).

In the developing tongue, taste bud primordia and papillae have been identified at GW9–GW10 by using electron microscopy (Hersch and Ganchrow, 1980). No markers of developing human taste buds are known. In order to visualize tongue papillae, we performed immuno-labeling with antibodies against Prox1 and Sox2, both of which control mouse taste bud differentiation (Nakayama et al., 2015, Okubo et al., 2006). Both Prox1 and Sox2 were detected in lingual papillae (including circumvallate papillae) covering the surface of the tongue (Figure S7B and S7C and **Movie S7**) in a similar pattern, suggesting that they are co-expressed in taste bud precursors, as observed in mice.

Whole-mount immunostaining for Sox2, which is known to be expressed by many types of cell progenitors (Sarkar and Hochedlinger, 2013), was also performed on other tissues from GW9.5, GW10, and GW12 fetuses. Strikingly, Sox2 expression was detected at the tip of each digit, in a narrow ring of cells lining the edge of the developing nails (Figure S7D and **Movie S7**). This indicates that Sox2 is a marker of fingernail stem cells in human fetuses, suggesting a role for this TF in nail development. Sox2 was also highly expressed in the ventricular zone of the developing brain (Figure S7E). Finally, we focused on the digestive system, which was collected in embryos and fetuses from GW7 to GW14 (n = 13). Staining with Sox9 clearly revealed the 3D organization of the developing villi of the gut epithelium where stem cells express this TF (Figure S7F and **Movie S7**) (Bastide et al., 2007). The enteric nervous system (ENS) has recently been the focus of many studies in part because of its frequent involvement in several genetic diseases (Heanue and Pachnis, 2007). ENS neurons are derived from neural crest cells, which colonize the gut around GW4. Double labeling for Phox2b (paired-like homeobox 2b) and Prph revealed the dense network of ENS neurons, which formed interconnected clusters covering the surface of the gut (Figure S7G and **Movie S7**). Prph staining also revealed the parasympathetic innervation of the digestive system (Figure S7G).

▼Conclusion

Here, we have combined immunolabeling with whole-body and whole-organ 3D imaging to provide a new comprehensive and unbiased method to study the early development of multiple human biological systems.

Non-invasive medical imaging of embryos and fetuses in utero has made remarkable progress. This includes 3D and 4D obstetrical ultrasonography that can generate holographic images of the embryo (Baken et al., 2015, Pooh et al., 2011) but mostly provides information about surface features and cavities, as well as 3D power Doppler, which visualizes the embryo vasculature (Weisstanner et al., 2015). In addition, in utero magnetic resonance imaging provides a good appreciation of the developing CNS in the fetus (Weisstanner et al., 2015) and diffusion tensor imaging (DTI) tractography is now used as a prenatal diagnostic of callosal dysgenesis as early as GW20 (Jakab et al., 2015). While these techniques represent valuable tools to visualize the gross anatomy of the fetus, they lack in resolution and are insufficient to resolve the molecular signature of individual cells or to know their organization within organs. Recently, whole-organ histology and 3D-reconstruction analysis based on the digital alignment of embryo sections has been performed (de Bakker et al., 2016), but it is extremely time consuming. Our method, which preserves the 3D organization of the organs while achieving a great cellular resolution, is rapid, highly reproducible, and should provide clinicians with a reliable spatial framework for the correlation of in utero and postmortem 3D images of embryos and fetuses.

The simplicity of this method, its robustness (for example, we could label endothelial cells in a fresh frozen GW5 embryo kept for 11 years at −80°C, unpublished data), and its sensitivity will facilitate its transfer to human embryology laboratories. Its use for the analysis of embryos and fetuses with genetic diseases and malformations will improve our understanding of their etiology.

Currently, the main limitations of our method are the availability of human embryos, the number of antibody combinations (a maximum of four at this time), the compatibility of the antibodies with our protocol (**Table S1**) and the storage of large size light-sheet image datasets. Nevertheless, the spectrum of future investigations and applications of this method in the field of embryology and fetology are countless. For instance, defining how many cells give rise to an individual organ and understanding how cell numbers are regulated during development is essential to understanding the process of organogenesis. Here, we show that whole-mount immunostaining with transcription factors and proliferation markers (KI67 and H3P) expressed in specific cell types (such as stem cells and muscle precursors) can be efficiently carried out in cleared embryos and fetal organs. This opens the possibility to obtain the number of cells expressing these factors, as well as map their localization in the body and estimate the rate of cell proliferation during the first trimester of human gestation—a critical period for various diseases in which tissue growth is perturbed. The recent surge of Zika virus infection and reports of its deleterious effects in the brain (Oliveira Melo et al., 2016) has demonstrated how incomplete our understanding of human embryo development is and how little we know about the mechanisms through which pathogens, toxins, and mutations impact embryogenesis. Our work shows that it should be possible in the near future to build a reference 3D atlas of the developing human. As a first step in this direction, all our 3D datasets are made available on a dedicated website (https://transparent-human-embryo.com/) that will also serve as a repository for additional embryology 3D data generated from our laboratory and others. This reference 3D atlas of the developing human and specific organs and systems not only represents a powerful educational online tool for researchers, educators, and students worldwide, but will allow 3D printing of anatomical models for didactic purposes in health sciences education programs.

▼Author Contributions

S.A.M., P.G., and F.C. collected, staged, and fixed the embryos and fetuses. M.B. and S.A.M. did the clearing and immunostaining. M.B. and D.G. performed the LSFM acquisitions and Imaris data processing. A.C. and M.B. did the figures. A.C., M.B., D.G., and G.C. analyzed the data. A.C. and P.G. wrote the manuscript. All authors corrected the manuscript.

▼Acknowledgments

We thank the midwives of the Gynaecology Department, Jeanne de Flandres Hospital of Lille (Centre d'Orthogénie), France, for their assistance and support. We also thank Robin Vigouroux, Reha Erzurumlu, and Peter Kozulin for correcting the manuscript, Yorick Gitton and Stéphane Fouquet (Institut de la Vision, Imaging Facility) for their help with the database, and Olivier Pourquié, Domna Karagogeos, William Stallcup, Carmen Birchmeier, and Jean-François Brunet for kindly providing some antibodies. Myog and Pax7 antibodies were obtained from the Developmental Studies Hybridoma Bank. We are also grateful to Olivier Pourquié, José Sahel,

Constantino Sotelo, and Nicole Le Douarin for helpful discussions. This work was supported by the Institut National de la Santé et de la Recherche Médicale (INSERM), France (grant number U1172), Agence Nationale de la Recherche (ANR), France (ANR-14-CE12-0015-01 to P.G., ANR-14-CE13-0004-01 to A.C.). It was performed in the frame of the LABEX LIFESENSES (reference ANR-10-LABX-65) supported by French state funds managed by the ANR within the Investissements d'Avenir programme under reference ANR-11-IDEX-0004-02.

▾ Supplemental Information

Table S1. Primary Antibodies Tested but Not Working with Our Protocol, Related to Figure 1

Movie S1. 3D Analysis of Human Cranial Nerve Development, Related to Figures 1 and S1

Movie S2. 3D Development of Hand and Foot Innervation, Related to Figures 2 and S1 and S2

Movie S3. 3D Imaging of the Developing Muscles, Related to Figures 3 and S3

Movie S4. 3D Imaging of the Developing Vasculature, Related to Figure 4

Movie S5. 3D Imaging of the Developing Cardiopulmonary System, Related to Figures 5 and S4

Movie S6. 3D Imaging of the Developing Urogenital System, Related to Figures 6, 7 and S5

Movie S7. 3D Analysis of Transcription Factor Expression in Human Embryos, Related to Figure S7

Received: November 18, 2016; Received in revised form: February 23, 2017; Accepted: March 3, 2017; Published: March 23, 2017
© 2017 Elsevier Inc.

Access this article on
ScienceDirect

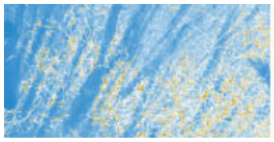
The Nemko Prize honors PhD-level work in Cellular or Molecular Neuroscience
Submit your nomination for this SfN award
CLICK HERE

Quick Links
About Cell Press
Advertisers
Recruitment Ads
Contact Us
Newsroom
Careers
Customer Service
Terms & Conditions
Privacy Policy
Use of Cookies
Mobile
Accessibility

Research Journals
Cancer Cell
Cell
Cell Chemical Biology
Cell Host & Microbe
Cell Metabolism
Cell Reports
Cell Stem Cell
Cell Systems
Chem
Current Biology
Developmental Cell
Immunity
iScience
Joule
Molecular Cell
Neuron
Structure

Reviews Journals: Trends In...
Biochemical Sciences
Biotechnology
Cancer
Cell Biology
Cognitive Sciences
Ecology & Evolution
Endocrinology & Metabolism
Genetics
Immunology
Microbiology
Molecular Medicine
Neurosciences
Parasitology
Pharmacological Sciences
Plant Science

Partner Journals
AJHG
Biophysical Journal
EBioMedicine
Heliyon
Molecular Plant
Molecular Therapy Family
Stem Cell Reports

Cell ISSN: 0092-8674

Copyright © 2018 Elsevier Inc. except certain content provided by third parties